Ao *et al. Soft Sci* 2024;4:3
DOI: 10.20517/ss.2023.34

Soft Science

Research Article

Open Access

Check for updates

A facile *in-situ* reaction method for preparing flexible Sb_2Te_3 thermoelectric thin films

Dongwei Ao[1,2,#], Bo Wu[3,#], Jabar Bushra[4], Bing Sun[5,*], Dong Yang[3], Yiming Zhong[3], Zhuanghao Zheng[3]

[1]School of Machinery and Automation, Weifang University, Weifang 261061, Shandong, China.
[2]School of Chemical Engineering and Technology, Tianjin University, Tianjin, 300072, China.
[3]Shenzhen Key Laboratory of Advanced Thin Films and Applications, Key Laboratory of Optoelectronic Devices and Systems of Ministry of Education and Guangdong Province, College of Physics and Optoelectronic Engineering, Shenzhen University, Shenzhen 518060, Guangdong, China.
[4]Institute for Metallic Materials, Leibniz Institute for Solid State and Materials Research Dresden (IFW Dresden), Dresden 01069, Germany.
[5]School of Physics and Electronic Information, Weifang University, Weifang 261061, Shandong, China.
[#]Authors contributed equally.

[*]**Correspondence to:** Bing Sun, School of Physics and Electronic Information, Weifang University, Dongfeng East Street, Weifang 261061, Shandong, China. E-mail: 20170005@wfu.edu.cn

How to cite this article: Ao D, Wu B, Bushra J, Sun B, Yang D, Zhong Y, Zheng Z. A facile *in-situ* reaction method for preparing flexible Sb_2Te_3 thermoelectric thin films. *Soft Sci* 2024;4:3. https://dx.doi.org/10.20517/ss.2023.34

Received: 30 Jul 2023 **First Decision:** 13 Sep 2023 **Revised:** 26 Sep 2023 **Accepted:** 30 Oct 2023 **Published:** 9 Jan 2024

Academic Editors: Zhifeng Ren, Takao Mori **Copy Editor:** Dong-Li Li **Production Editor:** Dong-Li Li

Abstract

Inorganic p-type Sb_2Te_3 flexible thin films (f-TFs) with eco-friendly and high thermoelectric performance have attracted wide research interest and potential for commercial applications. This study employs a facile *in-situ* reaction method to prepare flexible Sb_2Te_3 thin films by rationally adjusting the synthesized temperature. The prepared thin films show good crystallinity, which enhances the electrical conductivity of ~1,440 $S \cdot cm^{-1}$ due to the weakened carrier scattering. Simultaneously, the optimized carrier concentration, through adjusting the synthesis temperature, causes the intermediate Seebeck coefficient. Consequently, a high-power factor (16.0 $\mu W \cdot cm^{-1} \cdot K^{-2}$ at 300 K) is achieved for Sb_2Te_3 f-TFs prepared at 623 K. Besides, the f-TFs also exhibit good flexibility due to the slight change in resistance after bending. This study specifies that the *in-situ* reaction method is an effective route to prepare Sb_2Te_3 f-TFs with high thermoelectric performance.

Keywords: Thermoelectric, Sb_2Te_3, flexible thin film, thermal diffusion

INTRODUCTION

Thermoelectric (TE) technology can achieve direct conversion between thermal energy and electrical energy, which has significant applications in power generation and refrigeration[1-5]. With an increasing demand for micro-electromechanical systems of chip-sensors, wearable electronics, and implantable electronic devices, the TE flexible thin films (f-TFs) have attracted extensive interest due to their high adaptability to various conditions with high TE performance[6-10]. The TE performance of f-TFs can be accessed via power factor ($S^2\sigma$)[11], where σ and S represent the electric conductivity and Seebeck coefficient, respectively. Herein, σ is defined as $\sigma = n_h e\mu$, where n_h, e, and μ represent carrier concentration, elementary charge, and carrier mobility, respectively[12,13]. The S can be evaluated by Mott formula[14,15]. The increase of S can be achieved by the decreased n_h and increased effective mass (m^*). However, it is a significant challenge to simultaneously increase the S and σ due to their coupled relationship. Typically, f-TFs are composed of organic f-TFs and inorganic f-TFs[16,17]. For typical organic f-TFs, such as 3-hexylthiophene-2, 5-diyl ($FeCl_3$-doped P3HT, $S^2\sigma$ = ~0.2 μW·cm^{-1}·K^{-2} at 340 K)[18], carbon nanotubes/polyaniline (CNTs/PANI, $S^2\sigma$ = ~4.07 μW·cm^{-1}·K^{-2} at room temperature)[19], and poly (3,4-ethyl enedioxythiophene) polystyrene sulfonate (PEDOT/PSS, $S^2\sigma$ = ~3.34 μW·cm^{-1}·K^{-2} at room temperature)[20], a room temperature $S^2\sigma$ is lower than 5.0 μW·cm^{-1}·K^{-2}. Inorganic f-TFs, such as Ag_2Se ($S^2\sigma$ = ~18.6 μW·cm^{-1}·K^{-2} at room temperature)[21], SnSe ($S^2\sigma$ = ~3.5 μW·cm^{-1}·K^{-2} at 300 K)[22], Cu_2Se ($S^2\sigma$ = ~11.12 μW·cm^{-1}·K^{-2} at 549 K)[23], n-type Bi_2Te_3 ($S^2\sigma$ = ~14.65 μW·cm^{-1}·K^{-2} at room temperature)[24], p-type Sb_2Te_3 ($S^2\sigma$ = ~21.0 μW·cm^{-1}·K^{-2} at room temperature)[25], have been attracted great attention from the TE research community. It is evident that inorganic f-TFs approaches exhibited higher $S^2\sigma$ than that of the organic f-TFs, depicting good potential for commercial applications.

Among inorganic TE f-TFs, p-type Sb_2Te_3 f-TFs with a narrow bandgap of ~0.3 eV possess good TE performance at near room temperature[26]. So far, numerous methods have been employed to synthesize p-type Sb_2Te_3 f-TFs[27-32], such as thermal evaporation[29], magnetron sputtering[30], solution printing[31], and thermal diffusion[32]. Vieira *et al.* realized a high σ of ~320 S·cm^{-1} and $S^2\sigma$ of ~12.0 μW·cm^{-1}·K^{-2} at 298 K for Sb_2Te_3 f-TFs prepared by thermal evaporation[29]. Shang *et al.* successfully prepared (00*l*)-preferential orientation p-type Sb_2Te_3 f-TFs by magnetron sputtering methods and approached the σ of ~740 S·cm^{-1} and $S^2\sigma$ of ~12.4 μW·cm^{-1}·K^{-2} at 300 K. Sb_2Te_3 f-TFs prepared by screen-printing technology can approach σ of ~250 S·cm^{-1} and $S^2\sigma$ of ~14.3 μW·cm^{-1}·K^{-2} at room temperature[30,31]. It is concluded that the σ of Sb_2Te_3 f-TFs prepared by most of the preparation methods is lower than 1,000 S·cm^{-1} due to poor crystal growth. Consequently, the carrier transport properties were suppressed, and the corresponding TE performance of Sb_2Te_3 f-TFs is also limited.

In the present work, we employed a thermal diffusion method to prepare p-type Sb_2Te_3 f-TFs on a flexible polyimide (PI) substrate. The Sb and Te precursor films were deposited by thermal evaporation, as shown in Figure 1A. Pure Sb and Te f-TFs were obtained separately. The schematic diagram of the thermal diffusion process and the optical image of as-prepared Sb_2Te_3 f-TFs are shown in Figure 1B. The copper mold consists of a convex mold on the top and a concave mold placed below. Cu molds at both the top and bottom can enhance heat conduction and improve the uniformity of heat distribution during the thermal diffusion process. The Sb_2Te_3 f-TFs were synthesized by thermal diffusion methods using Te and Sb pure precursor films. The schematic diagram of the reaction process of Sb and Te during the thermal diffusion process is shown in Figure 1C. Through tuning the thermal diffusion temperature (T_{diff}), the Sb_2Te_3 f-TFs with standard stoichiometric ratios were obtained. Moreover, the moderate Seebeck coefficient of > 95 μV·K^{-1} was achieved at room temperature. Simultaneously, the μ and σ increased with increasing T_{diff} due to the weakened carrier scattering. Correspondingly, the highest value of $S^2\sigma$ of 16.0 μW·cm^{-1}·K^{-2} at T_{diff} = 623 K has been achieved. Besides, our prepared Sb_2Te_3 f-TFs approach good bending resistance.

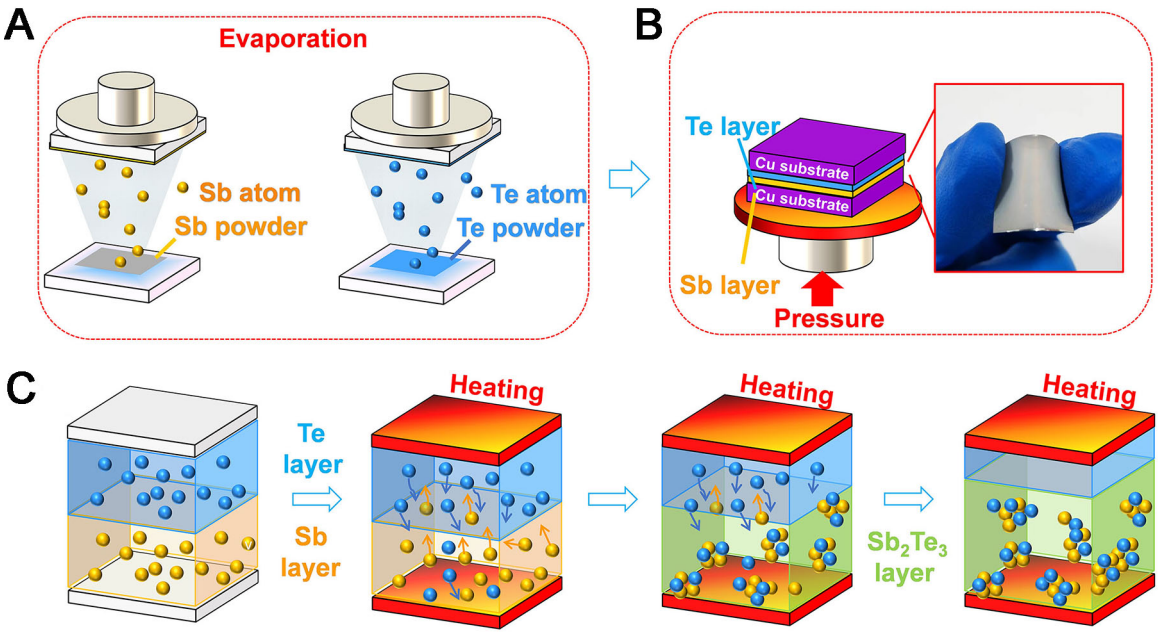

Figure 1. (A) The schematic diagram of the Sb and Te f-TFs prepared by thermal evaporation; (B) The schematic diagram of the thermal diffusion process. The Inset shows the optical image; (C) The schematic diagram of Sb_2Te_3 f-TF preparation through the thermal diffusion process. f-TFs: Flexible thin films.

EXPERIMENTAL

Sb_2Te_3 f-TF preparation process

The p-type Sb_2Te_3 f-TFs were prepared on a flexible PI substrate by a thermal diffusion method. First, Sb and Te films were deposited on PI substrates by using thermal evaporation. Te content is higher than a standard stoichiometric ratio of Sb:Te (2:3) due to the facile volatilization of Te induced by high saturation vapor pressure. The purity Sb (99.99 %) and Te (99.99 %) powders were weighed for 0.7025 and 1.5217 g, respectively. The Sb and Te evaporation parameters were as follows: the evaporation power of 18 and 20 W, the evaporation time of 13 and 16 min, and the evaporation pressure of 5×10^{-5} Torr, respectively, and the thickness of the Sb film and Te film were ~220 and ~520 nm. Secondly, the Te and Sb f-TFs were pressurized in the copper molds placed on heating equipment with a pressure of 1 N·mm^{-2}. The T_{diff} was set as 573, 603, 623, and 643 K, respectively. The corresponding heating and cooling rates are ~20 and 2 K/min, respectively. The sample was held at the target temperature for 30 min, and the pressurized sample was kept under vacuum for about 2 h to cool to room temperature. The as-prepared p-type Sb_2Te_3 f-TFs are shown in the inset of Figure 1B. The thickness of the as-prepared Sb_2Te_3 thin film is ~700 nm.

Characterization of the Sb_2Te_3 f-TFs

X-ray diffraction (XRD, D/max 2500 Rigaku Corporation, CuKα radiation) was employed to investigate crystal structures. Scanning electron microscopy (SEM) (Zeiss spra 55) and SEM with energy dispersive X-ray spectroscopy (SEM-EDS) (Bruker Quantax 200) were used to analyze the surface morphology and chemical composition of as-prepared Sb_2Te_3 f-TFs. Transmission electron microscopy (TEM) (FEI Tecnai G2 F20) and TEM-EDS (Bruker XFlash 5030) were also employed to study the crystal structure and chemical composition. X-ray photoelectron spectroscopy (XPS) was employed to measure the valence states of Sb and Te. The Geometric phase analysis (GPA) was further employed to analyze the lattice strains by the Strain++ software. A hall measurement system (HL5500PC, Nanometrics) was used to record the Hall performance. SBA458 (Nezsch) was used to measure the S and σ (error bars of 5% for S and 5% for σ).

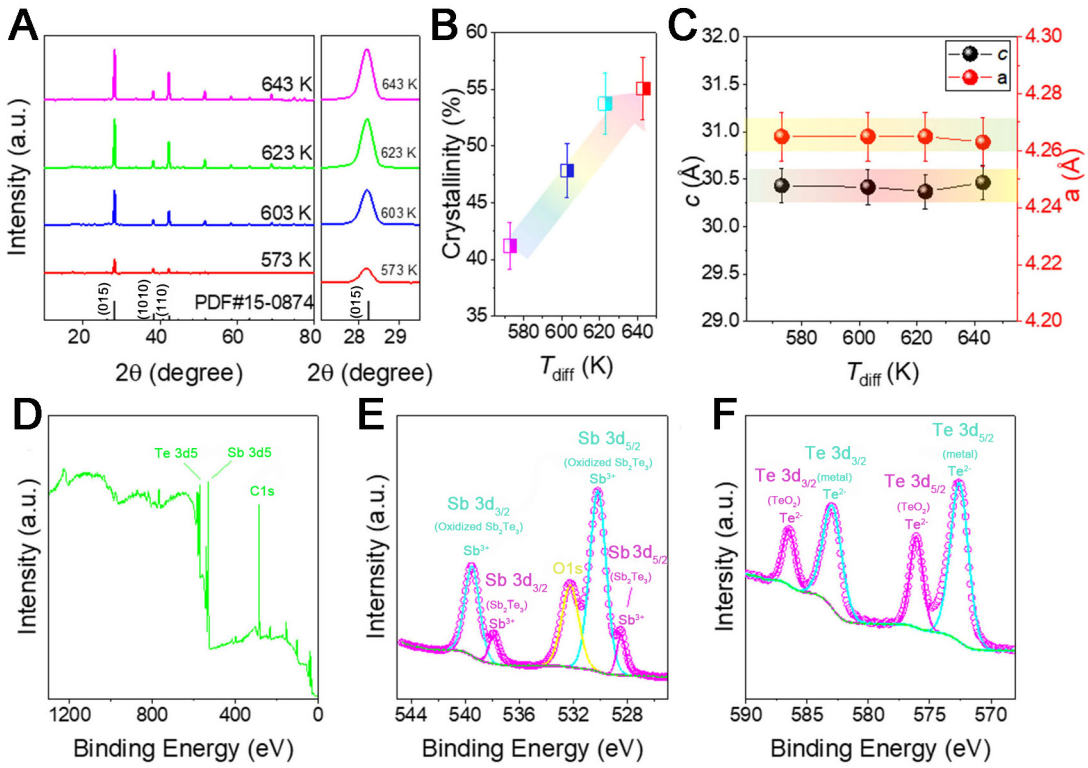

Figure 2. (A) The XRD spectra of as-prepared Sb_2Te_3 f-TFs; (B) The enlarged (015) peaks and the corresponding calculated crystallinity; (C) The lattice parameters; (D) The full XPS spectra; (E) and (F) XPS spectra of Sb and Te, respectively. f-TFs: Flexible thin films; XPS: X-ray photoelectron spectroscopy; XRD: X-ray diffraction.

RESULTS AND DISCUSSION

The crystal structure of Sb_2Te_3 f-TFs was investigated by XRD technology [Figure 2A]. All XRD peaks can be indexed to Sb_2Te_3 (PDF#15-0874), and no obvious impurity peaks were observed. The (015), (1010), and (110) diffraction peaks are the three main peaks. The highest peak is (015), indicating (015) preferred orientation of Sb_2Te_3 f-TFs. The enlarged (015) peaks are plotted in the inset I of Figure 2A, and the (015) peaks increased with increasing the T_{diff}. Further, the corresponding calculated crystallinity increased with increasing T_{diff} [Figure 2B]. Figure 2C depicts the calculated lattice parameters *a* and *c*, which clearly indicate the absence of any displacement in crystal structures. The valence states of Sb and Te in the Sb_2Te_3 films were investigated by XPS [Figure 2D-F]. Figure 2D-F presents the full XPS spectra and XPS spectra of Sb and Te, respectively. The presence of oxidized Sb_2Te_3 (indicated by peaks at 539.35 and 530.19 eV) and oxygen (evident in the O1s peak) is observed in Figure 2E due to the unencapsulated Sb_2Te_3 f-TFs used in an atmospheric environment. The binding energies at 528.46 and 537.77 eV were related to Sb $3d_{5/2}$ and Sb $3d_{3/2}$, respectively [Figure 2E], and the corresponding valance state of Sb was +3. The 3d core level of Te with two peaks at 586.54 and 576.99 eV was related to the oxidized Sb_2Te_3. Moreover, the binding energies at 583.03 and 572.82 eV are associated with Te $3d_{3/2}$ and Te $3d_{5/2}$, respectively [Figure 2F], and the corresponding valance state of Te is -2.

The crystal morphology and chemical composition of the as-prepared Sb_2Te_3 f-TFs were investigated through SEM and SEM-EDS technology [Figure 3]. Figure 3A shows the SEM surface morphology of Sb_2Te_3 f-TFs. All the films depict a morphology characterized by large particles, suggesting a typical dense polycrystalline structure. Figure 3B presents the EDS spectrum and atomic content of Sb_2Te_3 f-TFs prepared

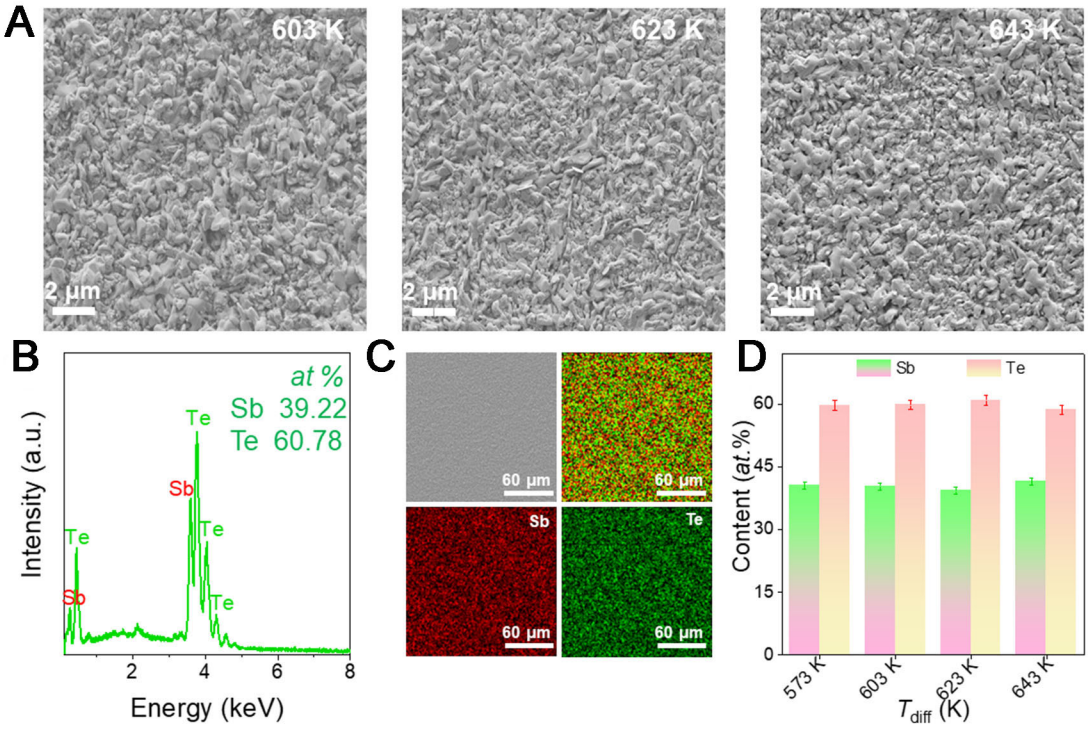

Figure 3. (A) SEM morphology of Sb_2Te_3 f-TFs prepared at T_{diff} = 603, 623, and 643 K, respectively; (B) EDS spectrum and atomic content of Sb_2Te_3 f-TFs prepared at T_{diff} = 623 K; (C) The corresponding SEM-BSE images and EDS maps; (D) The measured atomic contents of Sb_2Te_3 f-TFs. BSE: Backscattered electron; EDS: energy dispersive X-ray spectroscopy; f-TFs: flexible thin films; SEM: scanning electron microscopy.

at T_{diff} = 623 K. As can be seen, the chemical stoichiometry of Sb:Te was ~2.0:3.0. The corresponding EDS maps are shown in Figure 3C. Uniformly distributed Sb and Te elements were obtained, and no obvious enrichment in Te and Sb was detected. Figure 3C shows the atomic content of Sb_2Te_3 f-TFs, where the chemical stoichiometry of Sb:Te was closed to 2.0:3.0 for Sb_2Te_3 films prepared at T_{diff} from 573 to 623 K. When the T_{diff} reaches at 643 K, the chemical stoichiometry of Sb:Te was 2.0:2.8. It is suggested that the Te content slightly decreases due to the evaporation of Te at high temperatures.

To further study the changes in microstructure in detail, TEM was employed for the as-prepared Sb_2Te_3 f-TFs [Figure 4]. The low-resolution [Figure 4A] and high-resolution images [Figure 4B] for Sb_2Te_3 prepared at T_{diff} = 623 K show a neat arranged of lattices and the corresponding clear diffraction spots, which indicates good crystallinity of Sb_2Te_3 f-TFs. Figure 4C presents the enlarged image of the yellow square in Figure 4B. It can be seen that the measured value of the crystal spacing of ~3.2 Å can be indexed as the (015) plane of Sb_2Te_3, which was consistent with the XRD results. The lattice strains of Figure 4C are shown in Figure 4D and present no obvious lattice strain concentration along different directions due to the fewer lattice defects and lattice mismatches. In Figure 4E, the TEM-EDS maps depict that the Sb and Te are uniformly distributed throughout the Sb_2Te_3 nanoparticles. From the TEM-EDS [Figure 4F], it can be predicted that the chemical stoichiometry of Sb:Te is also close to 2.0:3.0 (at the nano-scale range).

As can be seen, Sb_2Te_3 thin films possess the highest $S^2\sigma$ near room temperature, as shown in Supplementary Figure 1. This work focuses on analyzing room-temperature TE performance as the core research topic. The TE performance of as-prepared Sb_2Te_3 f-TFs at room temperature is shown in Figure 5. The room temperature σ of Sb_2Te_3 f-TFs as a function of T_{diff} is shown in Figure 5A. The room temperature σ increased

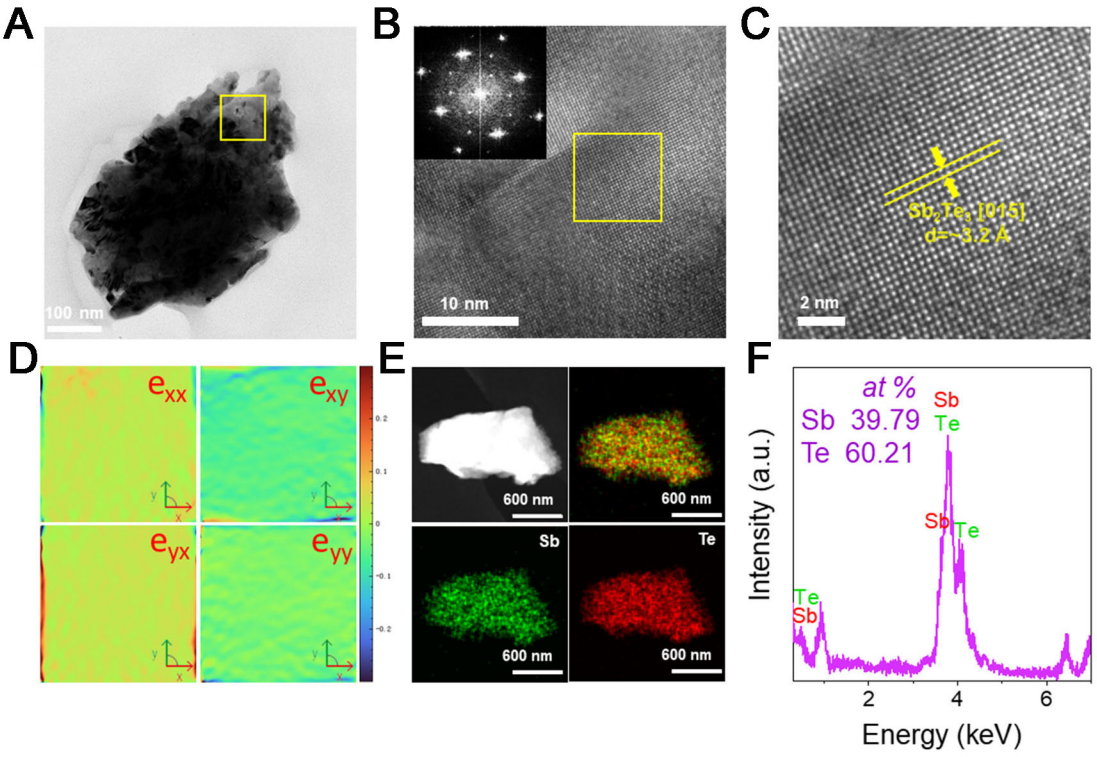

Figure 4. (A) Low-resolution TEM image of Sb_2Te_3 f-TF prepared at T_{diff} = 623 K; (B) High-resolution TEM image taken from the yellow square in Figure 4A; (C) The enlarged TEM images of the yellow square in Figure 4B; (D) The corresponding lattice strains of Figure 4C along different directions; (E) The TEM-EDS maps of Sb and Te; (F) The corresponding TEM-EDS spectrum. EDS: Energy dispersive X-ray spectroscopy; f-TFs: flexible thin films; TEM: transmission electron microscopy.

with increasing T_{diff}. Moreover, the highest value of σ reaches 1,440 S·cm^{-1} at T_{diff} = 643 K. To further study the changes of σ, we measured the μ and n_h of Sb_2Te_3 f-TFs at room temperature. Figure 5B compares the measured and calculated [based on single parabolic band (SPB)-model] μ as a function of n_h[33]. The μ increases with increasing T_{diff}, while the n_h varies from around 1.1 × 10^{19} cm^{-3}. It can be suggested that increasing μ is not mainly caused by the changes of n_h. The μ is achieved from 63.4 cm^2·V^{-1}·s^{-1} at T_{diff} = 573 K to a high value of 79.7 cm^2·V^{-1}·s^{-1} at T_{diff} = 643 K. In addition, the deformation potential coefficient (E_{def}) calculated by the SPB model roughly decreases with increasing T_{diff}. It is suggested that the enhanced crystallinity leads to the weakened carrier scattering, which is the main reason for the increased σ with increasing T_{diff}. Figure 5C presents the room temperature S as a function of T_{diff}. The positive values of S show the typical p-type semiconductor characteristics. Similar Seebeck coefficients are achieved due to all the films with a near standard stoichiometric ratio of 2:3. The S slightly increases and then decreases in the range of 95-110 μV·K^{-1} with increasing T_{diff}. The maximum S of ~106 μV·K^{-1} is achieved at T_{diff} = 623 K. The high Seebeck coefficient of as-prepared Sb_2Te_3 f-TFs is competitive with that of some bulk Sb_2Te_3[34]. Figure 5D shows the comparison between the measured and calculated S (based on the SPB model) as a function of n_h. As can be seen, the measured room temperature n_h remains nearly constant around 1.1 × 10^{20} cm^{-3} with increasing T_{diff}. Furthermore, the m^* calculated by the SPB model changed in the range from 1.26 to 1.37 m_0. Besides, the m^* increases and then decreases with increasing T_{diff}. Correspondingly, the trend of S with increasing T_{diff} is the same as the trend of m^*. The changes of S can be attributed to the changes of m^*. Figure 5E compares the measured $S^2\sigma$ and the calculated $S^2\sigma$ based on the SPB model at room temperature. All the $S^2\sigma$ value of Sb_2Te_3 f-TFs at room temperature is higher than 11 μW·cm^{-1}·K^{-2}. The maximum value of $S^2\sigma$ approaches as high as 16.0 μW·cm^{-1}·K^{-2} at T_{diff} = 623 K due to the high σ and moderate

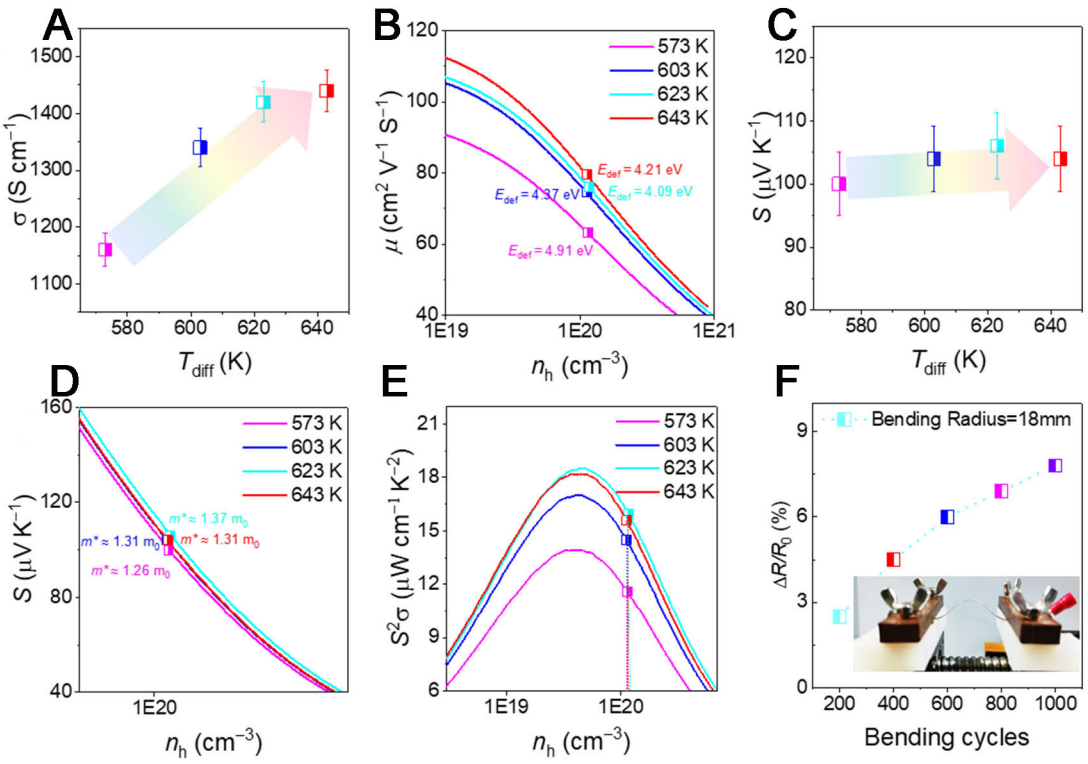

Figure 5. (A) The measured room temperature σ as a function of T_{diff}; (B) Comparison between the measured and SPB model calculated μ as a function of n_h; (C) The measured room temperature S as a function of T_{diff}; (D) Comparison between the measured and SPB model calculated S as a function of n_h; (E) Comparison between the measured $S^2\sigma$ and the calculated $S^2\sigma$ based on the SPB model at room temperature; (F) The R/R_0 and S/S_0 changes of Sb_2Te_3 with bending cycles of 1,000 and a bending radius of 18 mm. SPB: Single parabolic band.

S. The high $S^2\sigma$ of our prepared Sb_2Te_3 f-TFs is competitive with that of the reported Sb_2Te_3 f-TFs [Supplementary Table 1]. Herein, the prepared Sb_2Te_3 f-TFs possess high bending resistance. The high bending resistance of Sb_2Te_3 thin film is mainly attributed to the PI flexible substrate and Nano-scale thickness Sb_2Te_3 [35,36]. Both the resistance change ($\Delta R/R_0$) and Seebeck coefficient change ($\Delta S/S_0$) are lower than 10% under the bending cycles of 1,000 and bending radius of 18 mm [Figure 5F].

CONCLUSION

In this work, we successfully prepared Sb_2Te_3 f-TFs with high TE performance and bending resistance by the thermal diffusion method. Sb_2Te_3 f-TFs with standard stoichiometric ratios were achieved, which rationally tuned T_{diff} and increased the crystallinity of Sb_2Te_3 f-TFs. With increasing T_{diff}, tuning crystallinity increased σ and thus attenuated carrier scattering, achieving a high σ of ~1,440 S·cm^{-1} at T_{diff} = 643 K. The moderate S larger than 95 μV·K^{-1} has been achieved due to standard stoichiometric ratios of Sb_2Te_3 f-TFs. Correspondingly, an excellent room temperature $S^2\sigma$ of 16.0 μW·cm^{-1}·K^{-2} at T_{diff} = 623 K has been achieved. Besides, a $\Delta R/R_0$ of < 10% is achieved after 1,000 bending cycles with a bending radius of 18 mm, indicating good bending resistance.

DECLARATIONS

Authors' contributions

Made substantial contributions to the conceptualization and design of methodology and writing - original draft: Ao D, Wu B, Sun B, Yang D, Zhong Y

Performed data acquisition and technical work and provided supervision for writing - review and editing: Bushra J, Zheng Z

Availability of data and materials
Not applicable.

Financial support and sponsorship
This work was supported by Natural Science Foundation of China (12204355 and 52272210), Natural Science Fundations of Shandong Province (ZR2022QA018 and ZR2023ME001), the China Postdoctoral Science Foundation(2023M732609), and Doctoral Research Initiation Fund of Weifang University (2023BS01).

Conflicts of interest
All authors declared that there are no conflicts of interest.

Ethical approval and consent to participate
Not applicable.

Consent for publication
Not applicable.

REFERENCES
1. Liu D, Wang D, Hong T, et al. Lattice plainification advances highly effective SnSe crystalline thermoelectrics. *Science* 2023;380:841-6. DOI
2. Wu X, Han Z, Zhu Y, et al. A general design strategy for thermoelectric interface materials in n-type $Mg_3Sb_{1.5}Bi_{0.5}$ single leg used in TEGs. *Acta Mater* 2022;226:117616. DOI
3. Li Y, Lou Q, Yang J, et al. Exceptionally high power factor Ag_2Se/Se/polypyrrole composite films for flexible thermoelectric generators. *Adv Funct Mater* 2022;32:2106902. DOI
4. Chen YX, Zhang JZ, Nisar M, et al. Realizing high thermoelectric performance in n-type Bi_2Te_3 based thin films *via* post-selenization diffusion. *J Materiomics* 2023;9:618-25. DOI
5. Li L, Liu WD, Liu Q, Chen ZG. Multifunctional wearable thermoelectrics for personal thermal management. *Adv Funct Mater* 2022;32:2200548. DOI
6. Shi XL, Zou J, Chen ZG. Advanced thermoelectric design: from materials and structures to devices. *Chem Rev* 2020;120:7399-515. DOI PubMed
7. Zhang L, Shi XL, Yang YL, Chen ZG. Flexible thermoelectric materials and devices: from materials to applications. *Mater Today* 2021;46:62-108. DOI
8. Wang Y, Yang L, Shi XL, et al. Flexible thermoelectric materials and generators: challenges and innovations. *Adv Mater* 2019;31:1807916. DOI PubMed
9. Chi C, Liu G, An M, et al. Reversible bipolar thermopower of ionic thermoelectric polymer composite for cyclic energy generation. *Nat Commun* 2023;14:306. DOI PubMed PMC
10. Hu B, Shi XL, Zou J, Chen ZG. Thermoelectrics for medical applications: progress, challenges, and perspectives. *Chem Eng J* 2022;437:135268. DOI
11. Ao DW, Liu WD, Zheng ZH, et al. Assembly-free fabrication of high-performance flexible inorganic thin-film thermoelectric device prepared by a thermal diffusion. *Adv Energy Mater* 2022;12:2202731. DOI
12. Zhang R, Pei J, Han ZJ, Wu Y, Zhao Z, Zhang BP. Optimal performance of $Cu_{1.8}S_{1-x}Te_x$ thermoelectric materials fabricated via high-pressure process at room temperature. *J Adv Ceram* 2020;9:535-43. DOI
13. Shi X, Chen H, Hao F, et al. Room-temperature ductile inorganic semiconductor. *Nat Mater* 2018;17:421-6. DOI
14. Hashizume M, Yokouchi T, Nakagawa K, Shiomi Y. Anisotropic magneto-Seebeck effect in the antiferromagnetic semimetal $FeGe_2$. *Phys Rev B* 2021;104:115109. DOI
15. Hong M, Zou J, Chen ZG. Thermoelectric GeTe with diverse degrees of freedom having secured superhigh performance. *Adv Mater*

2019;31:1807071. DOI PubMed

16. Deng L, Liu Y, Zhang Y, Wang S, Gao P. Organic thermoelectric materials: niche harvester of thermal energy. *Adv Funct Mater* 2023;33:2210770. DOI
17. Wu Z, Zhang S, Liu Z, Mu E, Hu Z. Thermoelectric converter: strategies from materials to device application. *Nano Energy* 2022;91:106692. DOI
18. Wu L, Li H, Chai H, Xu Q, Chen Y, Chen L. Anion-dependent molecular doping and charge transport in ferric salt-doped P3HT for thermoelectric application. *ACS Appl Electron Mater* 2021;3:1252-9. DOI
19. Li H, Liu Y, Li P, Liu S, Du F, He C. Enhanced thermoelectric performance of carbon nanotubes/polyaniline composites by multiple interface engineering. *ACS Appl Mater Interfaces* 2021;13:6650-8. DOI PubMed
20. Fan Z, Li P, Du D, Ouyang J. Significantly enhanced thermoelectric properties of PEDOT:PSS films through sequential post-treatments with common acids and bases. *Adv Energy Mater* 2017;7:1602116. DOI
21. Gao Q, Wang W, Lu Y, et al. High power factor Ag/Ag_2Se composite films for flexible thermoelectric generators. *ACS Appl Mater Interfaces* 2021;13:14327-33. DOI PubMed
22. Rongione NA, Li M, Wu H, et al. High-performance solution-processable flexible snse nanosheet films for lower grade waste heat recovery. *Adv Elect Mater* 2019;5:1800774. DOI
23. Zheng ZH, Zhang DL, Jabar B, et al. Realizing high thermoelectric performance in highly (0*l*0)-textured flexible Cu_2Se thin film for wearable energy harvesting. *Mater Today Phys* 2022;24:100659. DOI
24. Ao DW, Liu WD, Chen YX, et al. Novel thermal diffusion temperature engineering leading to high thermoelectric performance in Bi_2Te_3-based flexible thin-films. *Adv Sci* 2022;9:2103547. DOI PubMed PMC
25. Wei M, Shi XL, Zheng ZH, et al. Directional thermal diffusion realizing inorganic Sb_2Te_3/Te hybrid thin films with high thermoelectric performance and flexibility. *Adv Funct Mater* 2022;32:2207903. DOI
26. Liu H, Li D, Ma C, et al. Van der Waals epitaxial growth of vertically stacked Sb_2Te_3/MoS_2 p-n heterojunctions for high performance optoelectronics. *Nano Energy* 2019;59:66-74. DOI
27. Ma F, Ao D, Liu X, Liu WD. Ti-doping inducing high-performance flexible p-type $Bi_{0.5}Sb_{1.5}Te_3$-based thin film. *Ceram Int* 2023;49:18584-91. DOI
28. Shen S, Zhu W, Deng Y, Zhao H, Peng Y, Wang C. Enhancing thermoelectric properties of Sb_2Te_3 flexible thin film through microstructure control and crystal preferential orientation engineering. *Appl Surf Sci* 2017;414:197-204. DOI
29. Vieira EMF, Figueira J, Pires AL, et al. Enhanced thermoelectric properties of Sb_2Te_3 and Bi_2Te_3 films for flexible thermal sensors. *J Alloys Compd* 2019;774:1102-16. DOI
30. Shang H, Li T, Luo D, et al. High-performance Ag-modified $Bi_{0.5}Sb_{1.5}Te_3$ films for the flexible thermoelectric generator. *ACS Appl Mater Interfaces* 2020;12:7358-65. DOI PubMed
31. Chang PS, Liao CN. Screen-printed flexible thermoelectric generator with directional heat collection design. *J Alloys Compd* 2020;836:155471. DOI
32. Zheng ZH, Shi XL, Ao DW, et al. Harvesting waste heat with flexible Bi_2Te_3 thermoelectric thin film. *Nat Sustain* 2023;6:180-91. DOI
33. Liu WD, Chen ZG, Zou J. Eco-friendly higher manganese silicide thermoelectric materials: progress and future challenges. *Adv Energy Mater* 2018;8:1800056. DOI
34. Shi J, Chen X, Wang W, Chen H. A new rapid synthesis of thermoelectric Sb_2Te_3 ingots using selective laser melting 3D printing. *Mater Sci Semicond Process* 2021;123:105551. DOI
35. Yang Q, Yang S, Qiu P, et al. Flexible thermoelectrics based on ductile semiconductors. *Science* 2022;377:854-8. DOI PubMed
36. Hollar C, Lin Z, Kongara M, et al. Flexible thermoelectrics: high-performance flexible bismuth telluride thin film from solution processed colloidal nanoplates (Adv. Mater. Technol. 11/2020). *Adv Mater Technol* 2020;5:2000600. DOI